Silver Nanowires for Plasmon Induced Enhancement of Optical Absorption in Thin-Film Silicon Solar Cells

Romain Mailhes*, Tetyana Nychyporuk**, Mustapha Lemiti *and* Vladimir Lysenko

Lyon Institute of Nanotechnology (INL), CNRS UMR 5270, Villeurbanne, F-69621, France
*romain.mailhes@insa-lyon.fr
**tetyana.nychyporuk@insa-lyon.fr

ABSTRACT

Plasmonic effects induced by silver nanocylinders embedded at rear side of a thin crystalline silicon (Si) substrate are reported. Numerical simulations were performed on a 3×3 nanowire array by means of 3D FDTD method. Absorption, scattering and extinction cross sections are calculated, and space distribution of absorbed power densities is computed. Up to 100 times enhanced absorbed power on nearly 70 % of the Si substrate is observed for a particular nanowire arangement. First experimental attempts devoted to fabrication of the simulated structures are also reported here.

Keywords: plasmonics, numerical simulations, nanowires, photovoltaics, absorption enhancement

1 INTRODUCTION

Thin-film silicon (Si) solar cells considered as a promising solution to reduce the costs of solar energy are only few microns thick. The reduced thickness of the active Si layers leads to a considerable weakness of general cell performances. In particular, light absorption becomes a critical factor strongly influencing the solar cell efficiency. Unfortunately, classical chemical treatments used to enhance the optical path of light in the case of thick solar cells are not suitable for the thin-film solar cells since the necessary surface roughnesses are of the same order of magnitude than the film thickness [1–3].

Plasmonics, which has seen a growing interest in the past few years, can provide several innovative ways for light absorption enhancement. Indeed, the collective coherent oscillation of free electrons in metallic nanostructures in resonance with an incident electromagnetic wave leads to new optical, magnetic and electrical properties which are very different from those of bulk metallic materials. These unique properties find numerous applications in various fields, such as: biology [4, 5], photonics, integrated optics [6], biosensors [7] and photovoltaics [8–10]. In particular, the plasmon-induced light scattering by metallic nanoparticles and near-field concentration of light ("hot-spots") are particularly attractive to be applied in photovoltaics [8, 9]. Indeed, they allow an enhancement of the absorption in a solar cell, and hence, an increase of its general efficiency [2,11–16]. Moreover, plasmonic peaks can be finely tailored by modifying: (i) geometrical aspects of the metal nanostructure assembly (shape, size, density) or (ii) materials properties, thus allowing enhancements in a wavelength range of special interest. In order to take all these parameters into account numerical simulations are required.

In this paper, numerical three-dimensional (3D) finite-difference time-domain (FDTD) simulations are firstly performed on a 3×3 nanowire array of silver (Ag) nanowires embedded at the rear side of a thin Si substrate. Various geometries are compared by varying location, size, and periodicity of the Ag array. Secondly, some experimental attempts devoted to fabrication of the simulated structures are also described.

2 NUMERICAL SIMULATIONS

Since there are a lot of different parameters controlling the surface plasmon resonance of an array of metallic nanostructures, a numeric simulation step is absolutely required in order to define the outlines of a particular attractive design with plasmon-enhanced properties. In this part of our paper, we describe the numerical simulations performed with 3D FDTD method using commercially available Lumerical solution package.

In order to especially enhance the light absorption in the near-infrared spectral region which is known to be extremely weak in the case of thin-film crystalline silicon solar cells, the Ag nanowires incorporated into the rear side of a Si thin film are considered. Indeed, noble metal nanostructures can exhibit a localised plasmon resonance in the near-infrared region [10, 17]. A general view of the simulated structure based on a 3×3 array of the Ag nanowires located at the rear side of a thin (1 μm) c-Si substrate is shown in the inset of Fig. 1. The simulation is performed with the use of Perfectly Matched Layer (PML) boundary conditions. A normally incident plane wave propagating along the z-axis and polarized along the x-axis is used to illuminate the simulated structure from its front side. Several configurations has been investigated by varying the diameter D and the periodicity P (edge-to-edge distance) of the Ag nanopillars.

For each considered structure, absorption, scatter-

CTSI-Cleantech 2013, www.ct-si.org, ISBN 978-1-4822-0594-7

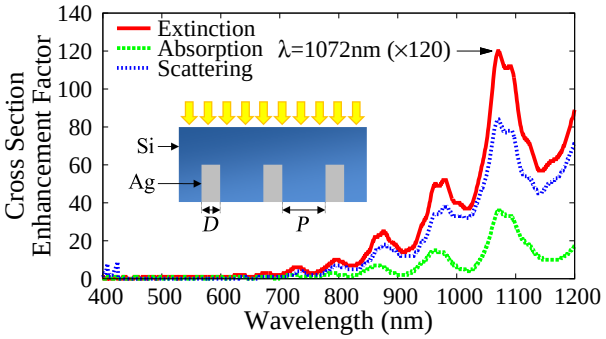

Figure 1: Calculated absorption, scattering and extinction cross-section enhancements for a simulated structure with $D = 100\,\text{nm}$ and $P = 250\,\text{nm}$. Inset shows a general view of the simulated structure.

ing and extinction cross-sections (respectively σ_{abs}, σ_{sca} and σ_{ext}, with $\sigma_{ext} = \sigma_{abs} + \sigma_{sca}$) has been calculated over the 400–1200 nm wavelength range. Silicon substrates both with and without (for comparison) metallic nanowires has been studied. Indeed, in order to bring to light the enhancements induced by the introduction of the nano-metal, the ratio of σ_{ext} for structure with cylinders over the bare Si one is calculated. For each considered structure a general enhancement is observed in the region of interest: $\lambda > 800\,\text{nm}$). Fig. 1 shows the cross-sections enhancements for a structure with $D = 100\,\text{nm}$ and $P = 250\,\text{nm}$. The maximum σ_{ext} enhancement, corresponding to the plasmonic peak for this configuration, is observed at $\lambda = 1072\,\text{nm}$.

Absorbed power density P_{abs} is then computed at the plasmon resonance wavelength deduced from the cross-sections calculations. Spatial mapping of the P_{abs} values allows us to identify the regions where the exciting radi-

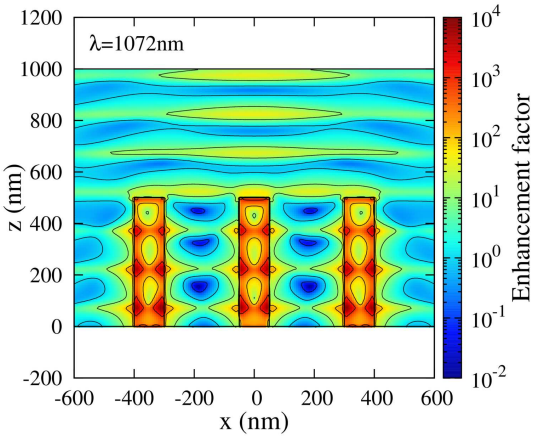

Figure 2: Mapping of the absorbed power density Pabs enhancement for $D = 100\,\text{nm}$ and $P = 250\,\text{nm}$. The wavelength corresponds to the maximum extinction cross-section enhancement ($\lambda = 1072\,\text{nm}$).

ation absorption is either improved (Enh. factor > 1) or reduced (Enh. factor < 1). For each considered structure a large part of the exciting light is absorbed within the metallic nanostructures. By aiming photovoltaic applications, we will consider the power absorbed in the Ag nanowires as lost, and we will focus our attention on the absorbed power within the Si thin films. The important scattering ability of the Ag nanowires can be easily deduced from the visible constructive and destructive interferences observed in Fig. 2. Hot-spots resulting from strong near-field coupling of the plasmon oscillations of neighbouring wires are not observed in the present structure since the distance between the pillars is quite important. Nevertheless, up to 100 times enhancement of the absorbed power takes place in nearly 70 % of the thin Si substrate volume.

3 EXPERIMENTAL

In order to experimentally verify the theoretical results described above, the Si substrates with the incorporated Ag nanowires have to be fabricated. An all-chemical method compatible with large-surface processing is investigated and some preliminary results are described below. The process flow-chart are schematically shown in Fig. 3.

3.1 Electrodeposition of Nanoparticles

First of all, in order to remove all impurities and native oxide, Si substrates are cleaned in a buffered oxide etch (BOE) solution for 10 s. The Si wafers are quickly rinsed and oxidized in an acidic piranha solution (4:1 mixture of concentrated H_2SO_4 and H_2O_2) for 10 mn, rinsed in ultra-pure water (UPW) for 10 mn and finally deoxidized in a 5 vol.% HF for 40 s. The cleaned Si substrates are then cleaved into $15\times15\,\text{mm}^2$ samples.

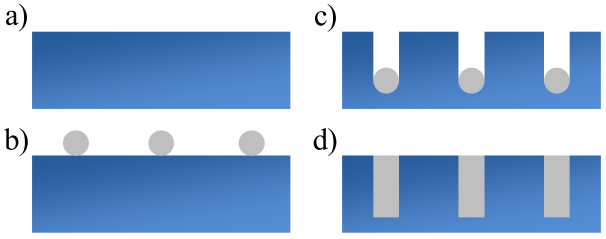

Figure 3: Schematic flow-chart of the plasmonic substrate fabrication: (a) Si substrate is cleaned to remove oxide and all kinds of impurities; (b) Ag nanoparticles are electrodeposited from a colloidal solution on top of the Si surface; (c) the nanoparticles catalyze local etching of Si leading to creation of pores with the Ag nanoparticles at their bottom; (d) the created pores are filled with Ag to create the nanowires.

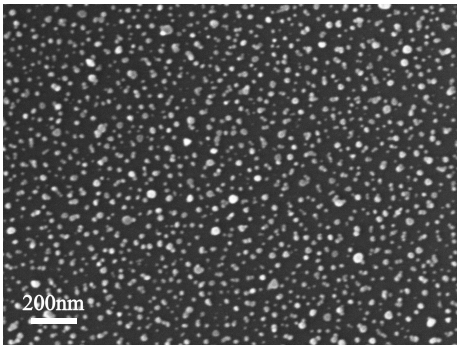

Figure 4: Plan-view scanning electron microscopy (SEM) image of the Ag nanoparticles ($D = 40\,\text{nm}$) electrodeposited on (100)-oriented Si substrate at a constant voltage $V = 40\,\text{V}$ for $t = 10\,\text{mn}$.

Ag colloidal nanoparticles stabilized in an aqueous buffer were purchased from Sigma-Aldrich. The nanoparticles were electrodeposited in a electrochemical cell on single crystalline (100)-oriented n-type Si wafers with a 1-20 Ωcm resistivity. Since the nanoparticles are stabilized with sodium citrate ions, they possess a negative charge at their surface when they are dispersed in polar liquids. The Si samples are put in direct contact with a copper (Cu) anode and a platinum-iridium (Pt-Ir) alloy cathode is set at an approximatively distance of 15 mm. The cell is filled with the colloidal solution of the Ag nanoparticles, and a constant voltage $V = 40\,\text{V}$ is applied for $t = 10\,\text{mn}$. Fig. 4 shows a plan-view scanning electron microscopy (SEM) image of the electrodeposited Ag nanoparticles without any visible aggregates. The SEM images are obtained with a MIRA FEG-SEM from TESCAN. The particles are strongly attached at the Si surface.

3.2 Metal-Assisted Chemical Etching

Metal-Assisted Chemical Etching (MACE) is a simple and low-cost method for the well controlled fabrication of Si nanostructures without size limitation. The basic principle is the following. A Si substrate loaded with noble metal is immersed in a acidic solution in presence of an oxidative agent. The catalytic activity of the noble metal induces the reduction of the oxidant. The generated holes resulting from this reaction then diffuse through the Ag nanoparticles and are injected into the substrate. Therefore, the Si in contact with the metal is oxidized, and dissolved by the acid. Since the concentration of holes is more important at the Ag/Si interface, the etching is faster beneath the particles, leading to an highly anisotropic etching along (100) direction [18]. The overall reaction proposed by Chartier *et al.* is:

$$\text{Si} + \frac{n}{2}\text{H}_2\text{O}_2 + 6\text{HF} \rightarrow n\text{H}_2\text{O} + \text{H}_2\text{SiF}_6 + \frac{4-n}{2}\text{H}_2 \uparrow \quad (1)$$

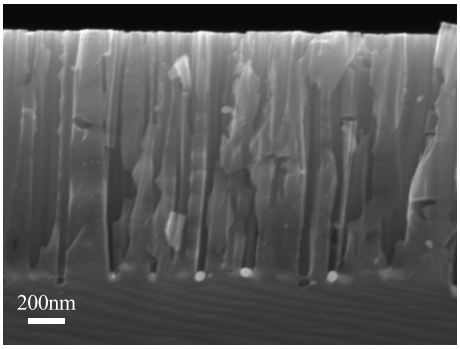

Figure 5: Cross-sectional SEM image of an n-type (100)-oriented Si substrate loaded with 60 nm Ag nanoparticles and etched at room temperature in $\text{HF}/\text{H}_2\text{O}_2/\text{H}_2\text{O}$ mixture for $t = 2\,\text{mn}$.

The morphology of the obtained porous nanostructures is mainly dependant on initial distribution of the noble metal nanoparticles at the surface of a Si wafer, on the surface conditions (noble metal in direct, and strong, contact with the substrate) and on the etching bath properties.

Our samples shown in Fig. 4 are immersed in a HF (5.3M)/H_2O_2 (0.18M)/H_2O etching mixture (25:10:4 volume ratio) for $t = 2\,\text{mn}$ at room temperature. In accordance with the MACE mechanisms described above, the perfectly spherical Ag nanoparticles sink into the Si substrate. The high proportion of the used acid compared to the oxidative agent ($\rho = [\text{HF}]/([\text{HF}] + [\text{H}_2\text{O}_2]) \simeq 97\%$) leads to the formation of straight cylindrical pores with diameter matching the Ag nanoparticles size (see Fig. 5) [19].

3.3 Pore Filling

Various methods for the pore filling with Ag, such as Ag electroless or electrolytic deposition are still under investigation. The major issue of such methods comes

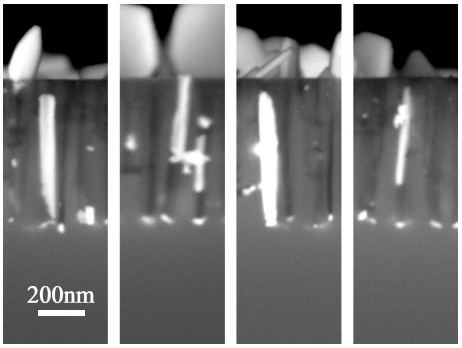

Figure 6: Cross-sectional SEM image of a sample after Ag electrolytic deposition. Partially filled and unfilled pores can be observed, as well as silver nanowires sticking up from the substrate.

CTSI-Cleantech 2013, www.ct-si.org, ISBN 978-1-4822-0594-7

from the non-negligible conductivity of the Si substrate. Thus, the Ag deposition inside the pores is not sufficiently favoured. This is confirmed by the first electrolytic deposition tests performed starting from the assumption that the Ag nanoparticles embedded at the bottom of the pores are much more conductive than the Si substrate. Ag is randomly deposited inside and outside the pores as shown by the observation of the filled and partially filled pores. An important part of the pores remain non-filled (Fig. 6).

4 CONCLUSIONS

In this communication, we have reported investigation of the plasmon-induced benefits ensured by adding the Ag nanowires inside a Si substrate. In presence of the Ag nanostructures, numerical simulations demonstrated a global enhancement of the absorbed power inside the Si thin layer. A particular design with strongly plasmon-enhanced absorption has been found. A chemical method for fabrication of plasmonic substrates with randomly arranged Ag nanoparticles is currently developed, and the first corresponding results have been reported. Once the key pore filling step will be mastered, further experiments dedicated to the organization of the cylinders will be carried out.

Acknowledgements

The experimental part of this work has been realized within the NanoLyon technological platform. The authors would like to gratefully acknowledge K. Ayadi, J. Gregoire and J.-L. Leclercq for training, support and fruitful discussions.

REFERENCES

[1] M. A. Green, Advances in Solar Energy 8, 231, 1993.

[2] S. Pillai, K. R. Catchpole, T. Trupke and M. A. Green, Journal of Applied Physics 101, 093105, 2007.

[3] F. J. Beck, A. Polman and K. R. Catchpole, Journal of Applied Physics 105, 114310, 2009.

[4] J. R. Lakowicz, Plasmonics 1, 5, 2006

[5] Y. Zakharko, T. Serdiuk, T. Nychyporuk, A. Géloën, M. Lemiti and V. Lysenko, Plasmonics 7, 725, 2012

[6] S. A. Maier, M. L. Brongersma, P. G. Kik, S. Meltzer, A. A. G. Requicha, B. E. Koel and H. A. Atwater, Advanced Materials 13, 1501 (2001).

[7] A.G. Brolo, Nature Photonics 6, 709 (2012).

[8] K. R. Catchpole and A. Polman, Optics Express 16, 21793, 2008.

[9] H. A. Atwater and A. Polman, Nature Materials 9, 205, 2010.

[10] S. Pillai and M. A. Green, Solar Energy Materials and Solar Cells 94, 1481, 2010.

[11] D. Derkacs, S. H. Lim, P. Matheu, W. Mar and E. T. Yu, Applied Physics Letters 89, 093103, 2006.

[12] C. Rockstuhl, S. Fahr and F. Lederer, Journal of Applied Physics 104, 123102, 2008.

[13] P. Matheu, S. H. Lim, D. Derkacs, C. McPheeters and E. T. Yu, Applied Physics Letters 93, 113108, 2008.

[14] R. A. Pala, J. White, E. Barnard, J. Liu and M. L. Brongersma, Advanced Materials 21, 3504, 2009.

[15] Y. A. Akimov, K. Ostrikov and E. P. Li, Plasmonics 4, 107, 2009.

[16] F. J. Beck, S. Mokkapati and K. R. Catchpole, Progress in Photovoltaics: Research and Applications 18, 500, 2010.

[17] U. Kreibig and M. Vollmer, "Optical Properties of Metal Clusters," Springer, 1995.

[18] Z. Huang, N. Geyer, P. Werner, J. de Boor and U. Gsele, Advanced Materials 23, 285, 2011.

[19] C. Chartier, S. Bastide and C. Lévy-Clément, Electrochimica Acta 53, 5509, 2008.